Compressed Sensing System Considerations for ECG and EMG Wireless Biosensors

Anna M. R. Dixon, *Student Member, IEEE*, Emily G. Allstot, *Student Member, IEEE*, Daibashish Gangopadhyay, *Member, IEEE*, and David J. Allstot, *Fellow, IEEE*

***Abstract*—Compressed sensing (CS) is an emerging signal processing paradigm that enables sub-Nyquist processing of sparse signals such as electrocardiogram (ECG) and electromyogram (EMG) biosignals. Consequently, it can be applied to biosignal acquisition systems to reduce the data rate to realize ultra-low-power performance. CS is compared to conventional and adaptive sampling techniques and several system-level design considerations are presented for CS acquisition systems including sparsity and compression limits, thresholding techniques, encoder bit-precision requirements, and signal recovery algorithms. Simulation studies show that compression factors greater than 16X are achievable for ECG and EMG signals with signal-to-quantization noise ratios greater than 60 dB.**

***Index Terms*—Biosignal sensors, body-area networks (BAN), compressed sensing (CS), compressive sampling, electrocardiogram (ECG), electromyogram (EMG), sparsity.**

I. Introduction

WEARABLE and wireless body-area networks (BAN) are revolutionizing healthcare [1]. As illustrated in Fig. 1, a BAN typically integrates multiple motion, inertial, and biosignal sensors with ultra-low-power radios. Real-time biomedical data is communicated to a BAN personal base station (e.g., a smartphone or personal computer) and then to a healthcare provider via the Internet. Increased energy efficiency is essential to the mass deployment of such feature-rich personal health-monitoring systems.

Most of the power in a biosignal sensor is dissipated when the RF power amplifier (PA) transmits data to the personal base station. For example, the PA in a BAN transmitter developed for the *Medical Implant Communications Service* (MICS) standard consumes 66.5 μW of the total power of 90 μW [2]. Thus, it is desirable to decrease the amount of data to be transmitted and reduce the duty cycle of the transmitter to increase the efficiency. C*ompressed sensing* (CS) does this. Specifically, the application of CS before the transmission of typical biosignals achieves compression of the data with a proportionate savings in energy. CS has been used previously to reduce noise and artifacts in ECG signals [3].

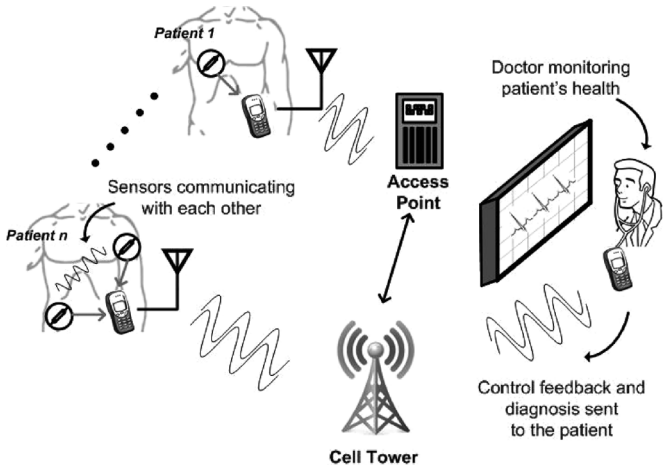

Fig. 1. Biosignal sensors communicate with a smartphone in a BAN to access a healthcare professional via the Internet.

Compressed sensing or compressive sampling is a data acquisition approach that requires only a few incoherent measurements to compress signals that are sparse in *some* domain [4]–[6]. For example, a typical ECG signal that comprises a high activity QRS *complex* followed by a low activity region between complexes (Fig. 2) is sparse in the time domain whereas EMG signals (Fig. 3) typically are sparse in the time and/or frequency domains [7]. In either case, CS compresses N input samples into $M(\ll N)$ output values. Simulation studies show that compression factors $> 16\times$ are possible for ECG [8] and EMG signals [9]. Hence, it is possible to reduce the duty cycle and the corresponding energy consumption of a BAN transmitter by the same factor.

In one possible embodiment of a CS CODEC, the transmitter [Fig. 4(a)] receives the biosignal from a low-noise amplifier. The analog front-end (AFE) compresses the N-sample analog input vector, $[X]$, into an M-sample analog output vector, $[Y]$. Consequently, the ADC and RF PA can operate with a smaller duty cycle. The receiver [Fig. 4(b)], which may reside in a smartphone, uses basis functions along with optimization techniques to recover the original signal.

Section II gives a brief history of the group sampling schemes that underpin CS followed by intuitive and mathematical descriptions of it. Section III compares CS to adaptive

Manuscript received August 03, 2011; revised November 19, 2011 and March 09, 2012; accepted March 27, 2012. Date of publication April 16, 2012; date of current version April 19, 2012. This work was supported by the National Science Foundation Contract EECS-0951368 and a grant from the Intel Corporation. A. M. R. Dixon was funded by a Ph.D. Graduate Fellowship and E. G. Allstot was funded by an Undergraduate Research Opportunity Scholarship from the Semiconductor Research Corporation. This paper was recommended by Associate Editor M. Stanaćević.

A. M. R. Dixon, E. G. Allstot, and D. J. Allstot are with the Department of Electrical Engineering, University of Washington, Seattle, WA 98195 USA (e-mail: allstot@uw.edu).

D. Gangopadhyay was with the University of Washington, Seattle, WA 98195 USA. He is now with Marvell Semiconductor Inc., Santa Clara, CA 95054 USA.

Color versions of one or more of the figures in this paper are available online at http://ieeexplore.ieee.org.

Digital Object Identifier 10.1109/TBCAS.2012.2193668

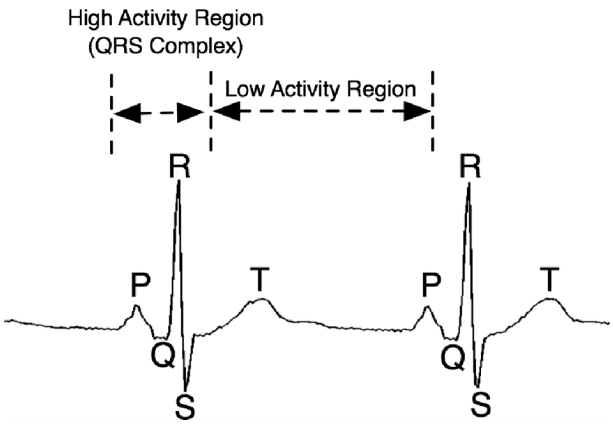

Fig. 2. A typical ECG waveform exhibits sparsity in the time domain.

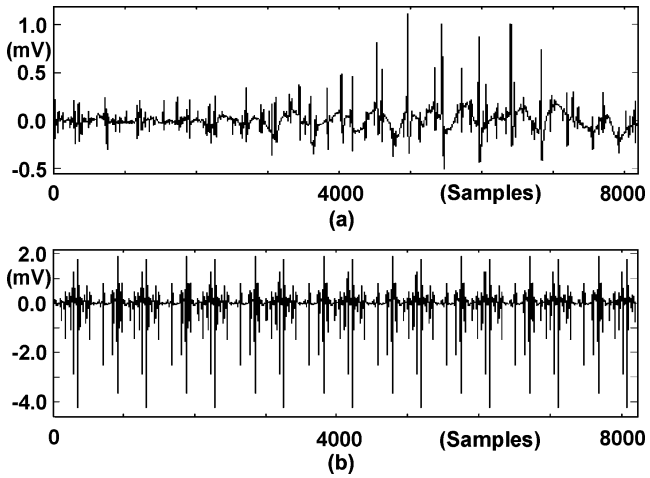

Fig. 3. Typical EMG biosignals exhibit sparsity in the time and/or frequency domains: (a) Healthy and (b) neuropathy [7]. $f_S = 4$ kHz.

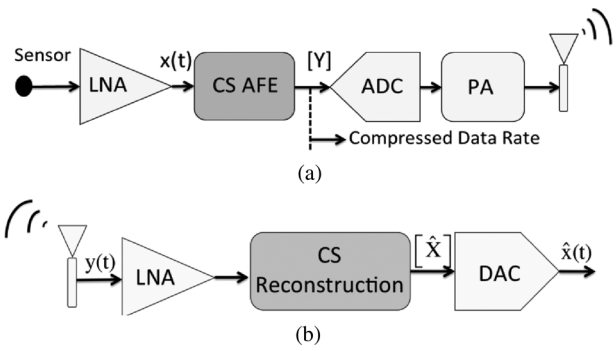

Fig. 4. An analog-based CS acquisition system. (a) The analog front-end in the ENCODER compresses the analog information prior to digitization and transmission. (b) The DECODER reconstructs the original signal.

sampling-based biosignal acquisition and Section IV describes biosignal dynamic thresholding techniques that are used to trade off the compression factor, C, (i.e., sparsity) against the signal-to-quantization noise ratio, $SQNR$, (i.e., accuracy). Practical design considerations for CS encoding and decoding are presented in Sections V and VI. Simulation studies are summarized for ECG and EMG biosignal sensors for BAN applications, and Section VII concludes the paper.

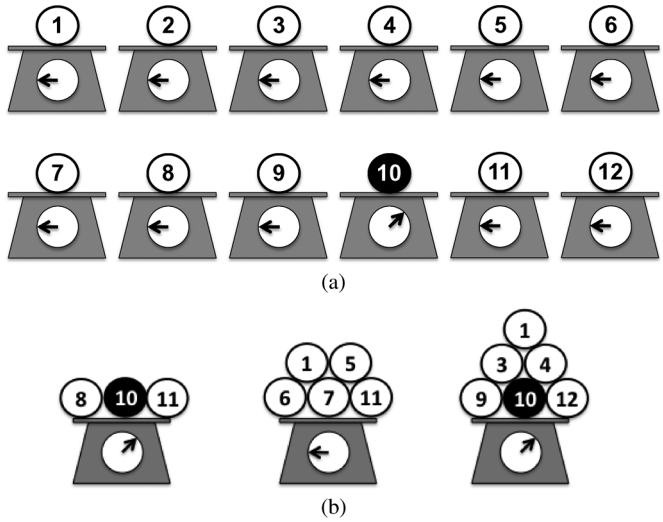

Fig. 5. (a) Conventional sampling. (b) Group sampling.

II. Compressed Sensing Background

During World War II when millions were conscripted into the U.S. military, the U.S. Public Health Service and Selective Service System engaged in a large-scale program to weed out syphilitic individuals. A blood sample was drawn from each prospective inductee and subjected to a Wasserman Test to detect a syphilitic antigen that is an indicator of the infection. However, such individual evaluation was precluded by the high cost and the urgency to get soldiers to the battlefield as quickly as possible. These drawbacks were overcome using the *group testing* techniques introduced in the landmark paper by Dorfman [10]. He proved that pooling the blood samples from a group of inductees and performing a single test was viable because the probability of syphilis was small (i.e., the "signal" was sparse). Obviously, it was more economical to test groups rather than all of the individuals. The group testing concept was extended by Sobel and Groll in component testing at the Bell Telephone Company [11]. The seminal ideas in these papers underpin compressed sensing.

A. An Intuitive View of CS

Imagine an experiment with many objects in which only one element is "different" (i.e., the signal is *sparse*). The goal is to identify the sparse object(s) with minimal effort. In traditional testing, each object is measured individually. In group testing, the large difference between the total number of objects in the set and the number of different objects is exploited by examining only a few groupings. Consequently, the sparse object is found with fewer tests.

The traditional and group testing techniques are compared in Fig. 5. In this puzzle, there is a set of 12 balls wherein one is much heavier (100 g) than the others (1 g). The objective is to identify the heavy ball (Ball #10, the black ball). In order to present an appropriate analogy to the acquisition of a sparse signal and the application of compressed sensing, the measurement protocol is assumed to be non-adaptive. That is, once the measurement process has commenced, it will not cease until completed even upon obvious identification of the heavy ball.

The traditional sampling method [Fig. 5(a)] weighs each ball separately. The corresponding matrix representation is

$$\begin{bmatrix} 1\,\mathrm{g} \\ 1\,\mathrm{g} \\ 1\,\mathrm{g} \\ 1\,\mathrm{g} \\ 1\,\mathrm{g} \\ 1\,\mathrm{g} \\ 1\,\mathrm{g} \\ 1\,\mathrm{g} \\ 1\,\mathrm{g} \\ 100\,\mathrm{g} \\ 1\,\mathrm{g} \\ 1\,\mathrm{g} \end{bmatrix} = \begin{bmatrix} 1&0&0&0&0&0&0&0&0&0&0&0 \\ 0&1&0&0&0&0&0&0&0&0&0&0 \\ 0&0&1&0&0&0&0&0&0&0&0&0 \\ 0&0&0&1&0&0&0&0&0&0&0&0 \\ 0&0&0&0&1&0&0&0&0&0&0&0 \\ 0&0&0&0&0&1&0&0&0&0&0&0 \\ 0&0&0&0&0&0&1&0&0&0&0&0 \\ 0&0&0&0&0&0&0&1&0&0&0&0 \\ 0&0&0&0&0&0&0&0&1&0&0&0 \\ 0&0&0&0&0&0&0&0&0&1&0&0 \\ 0&0&0&0&0&0&0&0&0&0&1&0 \\ 0&0&0&0&0&0&0&0&0&0&0&1 \end{bmatrix} \times \begin{bmatrix} 1\,\mathrm{g} \\ 1\,\mathrm{g} \\ 1\,\mathrm{g} \\ 1\,\mathrm{g} \\ 1\,\mathrm{g} \\ 1\,\mathrm{g} \\ 1\,\mathrm{g} \\ 1\,\mathrm{g} \\ 1\,\mathrm{g} \\ 100\,\mathrm{g} \\ 1\,\mathrm{g} \\ 1\,\mathrm{g} \end{bmatrix}$$

That is, the *output vector* $[Y]$ equals the *measurement matrix* $[\Phi]$ times the *input vector* $[X]$. $[\Phi]$ defines the measurement protocol which is an identity matrix $[I]$ in this case because only one ball is measured at a time. Thus, traditional sampling requires N measurements for N balls.

CS is applied to the 12-ball problem using the $[\Phi]$ matrix below wherein *random groups* of balls are measured as depicted in Fig. 5(b). CS works well for such problems where the "signal" is sparse.

$$\begin{bmatrix} 102\,\mathrm{g} \\ 5\,\mathrm{g} \\ 105\,\mathrm{g} \end{bmatrix} = \begin{bmatrix} 0&0&0&0&0&0&0&1&0&1&1&0 \\ 1&0&0&0&1&1&1&0&0&0&1&0 \\ 1&0&1&1&0&0&0&0&1&1&0&1 \end{bmatrix} \times \begin{bmatrix} 1\,\mathrm{g} \\ 1\,\mathrm{g} \\ 1\,\mathrm{g} \\ 1\,\mathrm{g} \\ 1\,\mathrm{g} \\ 1\,\mathrm{g} \\ 1\,\mathrm{g} \\ 1\,\mathrm{g} \\ 1\,\mathrm{g} \\ 100\,\mathrm{g} \\ 1\,\mathrm{g} \\ 1\,\mathrm{g} \end{bmatrix}$$

For sparse signals, a few measurements of random groupings accurately capture the essential information with high probability. $[\Phi]$ comprises coefficients sampled from a random probability distribution function (pdf) such as Gaussian, Uniform, etc. The 1-bit random coefficients above are from a Bernoulli pdf where 0(1) represents the absence (presence) of a specific ball. In this example, CS reduces the total number of measurements by $4\times$ even though the sparsity level is only $11/12 = 91.7\%$. Simulations show that ECG and EMG signals can be compressed up to $16\times$ [8], [9].

A decoder [Fig. 4(b)] receives the compressed vector $[Y]$ and reconstructs the original signal. It deduces from only three measurements that Ball #10 is the heavy ball because it is the only commonality between the two heavy groupings.

B. Formal Definition of Compressive Sampling

Representative signals for the CS system of Fig. 4 for a typical ECG biosignal (thresholded to reduce baseline drift and noise) after acquisition, compression, and reconstruction are shown in Fig. 6. The analog input vector, $[X]$, comprises 1024 samples and the compressed analog output vector, $[Y]$, has 256 samples.

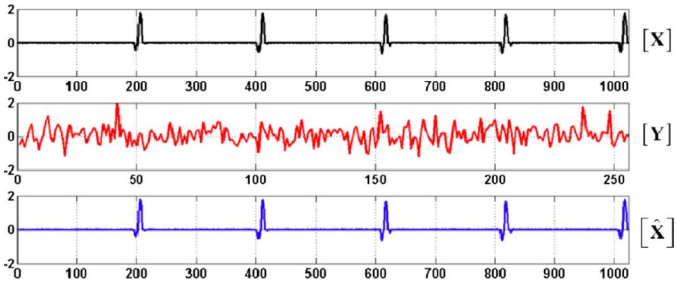

Fig. 6. A thresholded ECG signal before, $[X]$, and after CS compression, $[Y]$, and after reconstruction, $[\widehat{X}]$.

Optimization algorithms are used in the decoder to reconstruct the input vector $[\widehat{X}]$.

Compressed sensing is the *non-adaptive* sampling scheme embodied in the matrix equation

$$[Y] = [\Phi][X] \tag{1}$$

where $[X]$ is the input vector of length N, $[Y]$ is the compressed vector of length M, and $[\phi]$ is the $M \times N$ *measurement* or *sensing matrix*. CS is considered non-adaptive because $[\phi]$ remains constant. In many cases, an effective input vector is defined as

$$[X] = [\psi][\alpha] \tag{2}$$

where $[\alpha]$ is the original N-sample input vector and $[\psi]$ is the $N \times N$ *sampling basis* or *sparsifying matrix*. For example, if the original signal is sparse in the frequency domain, $[\psi]$ is populated with Fourier coefficients, whereas $[\psi]$ is simply an identity matrix if $[\alpha]$ is sparse in the time domain.

CS captures M measurements from N samples according to (1) using random linear projections [4]–[6]. The attraction of CS for ultra-low power implementations of biosignal sensors follows from the data compression factor

$$C = \frac{N}{M}. \tag{3}$$

Two requirements enable an efficient implementation.

1) The input signal, $[X]$, is sparse in some domain.
2) The sampling basis, $[\psi]$, and the measurement matrix, $[\phi]$, are *incoherent*.

$[X]$ is sparse when only a few elements in $[\alpha]$ are significant and $[\psi]$ determines the domain of sparsity. For time-domain sparse signals ($[\psi] = [I]$), if K elements of $[X]$ are greater than the other $N-K$ elements, only the K largest elements are kept in $[X_K]$; i.e., the signal is thresholded. A definition of sparsity is

$$Sparsity\,(\%) = (1 - K/N) \times (100\%). \tag{4}$$

Sparsity control by thresholding is advantageous when $[X]$ is well approximated by $[X_K]$; that is, the *L2-norm* of the residue, $\|X - X_K\|_2$, is small. For accurate and numerically stable compression and reconstruction, Candès recommends [6]

$$M > C_k K \log\left(\frac{N}{K}\right) \tag{5}$$

where C_k is an empirical constant. (5) limits the maximum achievable compression for a given sparsity level.

Studies have shown that a common characteristic of biosignals is sparsity in some basis. For example, an ECG signal (Fig. 2), which comprises a high activity QRS complex followed by a long period of low activity between complexes, is sparse in the time domain, whereas EMG signals (Fig. 3) are sparse in the time and/or frequency domains.

Incoherence guides the formulation of the measurement matrix. Incoherence between $[\psi]$ and $[\phi]$ is needed to whiten the measurements to ensure capture of the key characteristics of the signal. Thus, a sparse signal in the $[\psi]$ domain [Fig. 6(a)] appears as a dense noise-like compressed signal, $[Y]$ [Fig. 6(b)]. It is fortunate that random matrices are, with high probability, highly incoherent with any fixed basis $[\psi]$ [4]–[6]. Thus, the measurement matrix can be populated with random values from many different probability density functions.

Accurate and efficient signal recovery is central to the implementation of a CS system. Ideally, reconstruction can be posed as solving $[Y] = [\phi][\hat{X}]$ However, there are N unknown values in the reconstructed signal, $[\hat{X}]$, but only M known values in the measured signal, $[Y]$. Hence, the problem is under-determined with many possible solutions because $[\phi]$ is non-square and non-invertible. A solution is achievable, however, because $[\hat{X}]$ must be sparse which greatly reduces the set of possibilities which facilitates optimization. The L_1-*norm* is a measure of sparsity; hence, the following minimization defines a CS signal recovery:

$$Min\|\hat{X}\|_1 \quad \text{subject to} \quad [Y] = [\Phi][\hat{X}]. \tag{6}$$

The sparsity and incoherence constraints ensure, with high probability, that the solution to (6) is exact; i.e., $[\hat{X}] = [X]$.

III. Compressive Versus Adaptive Sampling

Conventional ECG monitoring systems use a constant sampling rate (e.g., 256 Hz) as determined by the *rate of change* of the signal in the QRS complex (Fig. 2). Hence, high frequency information is captured but unnecessary oversampling is performed during the low-activity periods.

Adaptive sampling adjusts f_S to the activity level [12], [13] as illustrated in Fig. 7 for an ECG signal. Its implementation differs from that of CS as summarized in Table I. An activity detection algorithm and circuit are needed to identify the high frequency regions of the signal and adjust the sampling rate accordingly [13]; specifically, the sampling rate is low, f_l, or high, f_h, as shown. Thus, the effective digitization rate is

$$f_{s,eff} = x f_{s,h} + (1 - x) f_{s,l} \tag{7}$$

where x, the fraction of time when the high signal activity is detected, is tuned based on the desired level of detail. Hence, the signal is sampled at a lower effective rate which maintains adequate accuracy and reduces energy consumption. The digitization rate for CS is a fixed fraction of the Nyquist rate as determined by the compression factor

$$f_{s,eff} = f_s \left(\frac{M}{N} \right). \tag{8}$$

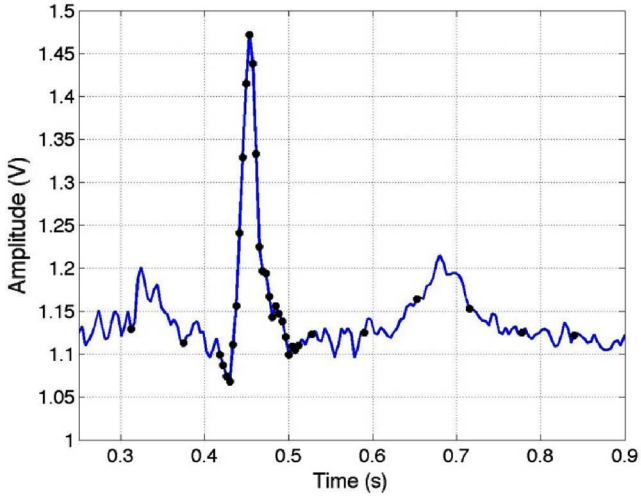

Fig. 7. Adaptive sampling applied to an ECG biosignal.

TABLE I
ADAPTIVE VERSUS COMPRESSIVE SAMPLING

	Adaptive Sampling	**Compressive Sampling**
Sampling Rate	$f_{s,eff} = xf_{s,h} + (1\text{-}x)f_{s,l}$	$f_{s,eff} = (M/N)f_s$
A-priori Knowledge	Yes	No
Additional Sensor Circuitry	Activity Detection Circuit and Sampling Control Mechanism	Thresholding Circuit

Adaptive sampling requires a priori knowledge of the signal which limits its versatility whereas CS is universally applicable to ECG, EMG, electroencephalogram (EEG), etc.

A final consideration relates to the hardware differences between the two approaches. Adaptive sampling requires activity detection circuitry (e.g., a differentiator and a comparator [13]) along with a microcontroller to tune it. CS requires thresholding circuitry (Section IV) to enable a tradeoff between sparsity (i.e., level of detail) and compression (i.e., energy efficiency). An alternative input-feature correlated asynchronous approach was recently presented by Hwang *et al.* [30] and Agarwal *et al.* [31].

IV. Sparsity Control and Thresholding

The compression factor of CS can be varied by controlling the sparsity $[K/N$ in (5)] of the input signal. This gives the healthcare professional a mechanism to control the level of detail (Fig. 1). Ambulatory quality monitoring requires the acquisition of relatively coarse features such as heart-rate, sudden body movements (EMG peaks), etc. Conversely, when an event of clinical significance is detected such as a sudden drop in the heart-rate, etc., a signal can be fed back from the Doctor to increase the level of accuracy to diagnostic quality. Greater detail during diagnostic evaluation means reduced compressibility and reduced overall energy efficiency.

Sparsity control is accomplished by a careful selection of the sparsifying domain (2), which is application dependent,

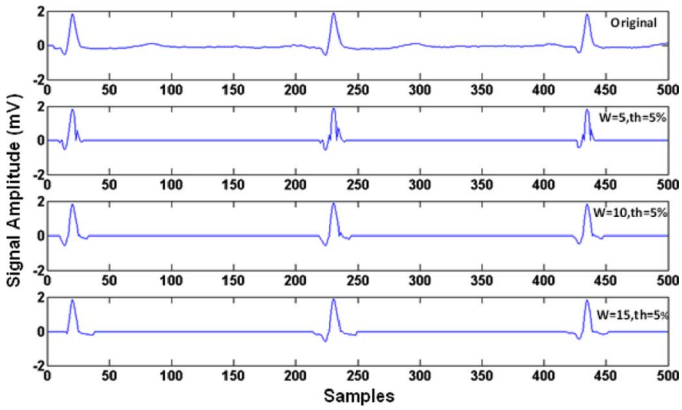

Fig. 8. A healthy ECG signal before and after dynamic thresholding with averaging window lengths of $W = 5$, 10, and 15 samples and $th = 0.05$.

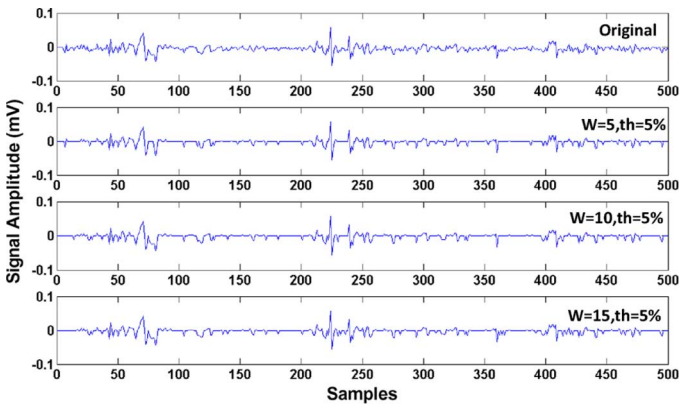

Fig. 9. A healthy EMG signal before and after dynamic thresholding with averaging window lengths of $W = 5$, 10, and 15 samples, and $th = 0.05$.

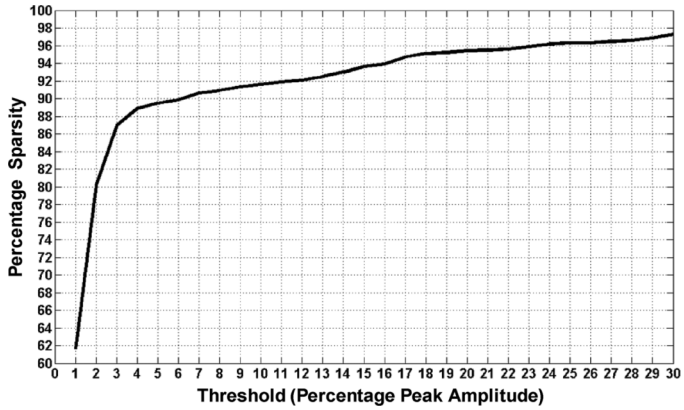

Fig. 10. Sparsity versus threshold level for a healthy ECG signal (Fig. 8); $W = 10$.

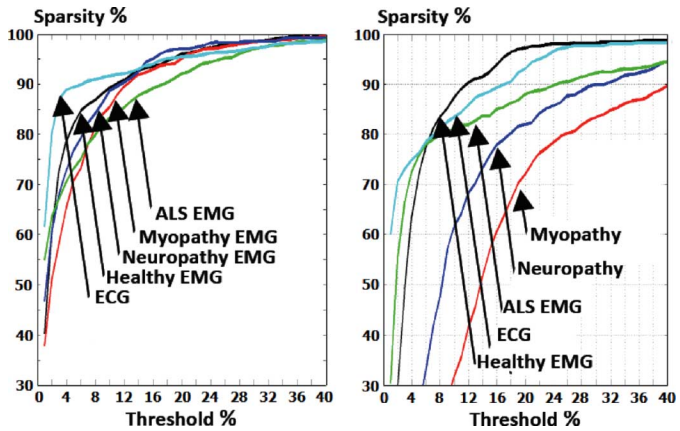

Fig. 11. Sparsity versus threshold level for Physiobank EMG and ECG signals [7] with $W = 5$ (left) and 10 (right). ALS is Amyotrophic Lateral Sclerosis—Lou Gehrig's disease.

followed by thresholding. Thresholding increases sparsity by selecting only the larger signal amplitudes (in the sparsifying domain) to be processed. Two common techniques are absolute and dynamic thresholding. In the former, the sample value is compared to a predefined threshold level to determine if it should be processed whereas in the latter, the sample value is compared to a local average of the signal. Dynamic thresholding was proven previously as an effective technique for neural spike detection [14]; herein it is used with ECG and EMG signals to increase sparsity and thus compressibility.

The first step in dynamic thresholding is to track the DC level of the signal by computing a sliding average over a window of length, W, which accounts for baseline drifts, DC offsets, etc. The threshold level, th, is then set to a fraction of the peak-to-peak amplitude. If the magnitude of the next input sample is $> th$, it is processed as is; if it is $< th$, it is set to zero. Thus, the positive and negative signal peaks are maintained while small sample values are set to zero.

Dynamic thresholding addresses the challenge of careful tuning in CS to maximize signal sparsity and minimize distortion; W and th are the critical performance parameters. Broad peaks are not detected if W is too short, whereas information below the DC level is lost if W is too long. Hence, W should be determined from the period between signal peaks. Figs. 8 and 9 show that $W = 10$ (ECG) and $W = 5$ (EMG) work well based on experiments on several hours of clinical data [7]. Fig. 10 plots ECG sparsity versus th and Fig. 11 compares ECG and EMG sparsity levels versus th.

V. Design Considerations for the CS Encoder

A CS ENCODER computes the compressed output vector $[Y] = [\phi][X]$. This section considers implementation issues including the design of the measurement matrix.

A. CS Encoder Architecture

The implementation issues and performance characteristics of two analog-domain CS architectures intended for spectral estimation (e.g., cognitive radios) and an integrated digital-domain CS system with applications to ECG and EEG biosignals are described in this section.

Laska *et al.* [15] presented an analog-domain CS system—random demodulation (RD) [Fig. 12(a)]—and applied it to sparse multi-tone signals. The RD system first mixes the analog signal, $[X]$, with a random signal, $[\phi]$, using a Gilbert multiplier. The resulting signal is then integrated over M successive windows using an active RC integrator, and the output, $[Y]$, is digitized by an ADC. $HSPICE$ simulations

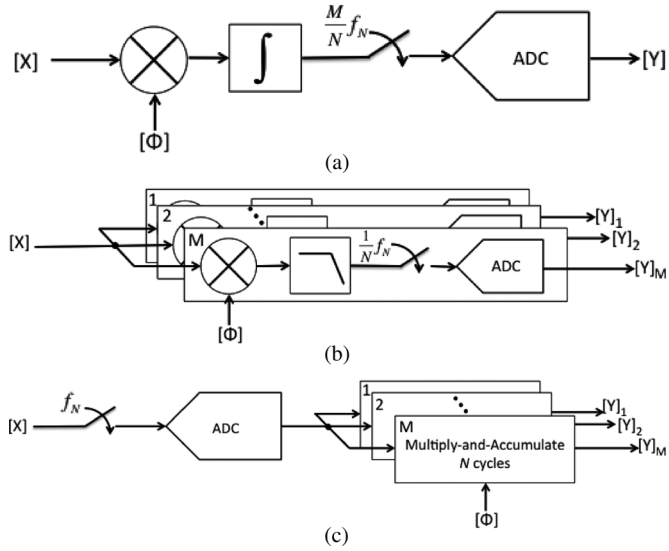

Fig. 12. Prior compressed sampling architectures. (a) Random demodulation [15], [16]. (b) Modulated wideband converter [17]. (c) Digital CS [18].

using 0.13 μm CMOS device models demonstrated a sampling rate 6× less than the Nyquist rate for an AM signal with three tones. The approach was subsequently validated in a hardware prototype by Ragheb *et al.* [16]. Measurements for the same three-tone AM input signal showed SNR values of 45.5 dB, 42.9 dB and 39.6 dB for sampling frequencies of 1/2, 1/4 and 1/8 of the Nyquist rate, respectively.

Mishali *et al.* [17] proposed another analog-domain CS system—a modulated wideband converter (MWC) [Fig. 12(b)]—for the compression of sparse multiband signals. In MWC, N samples, $[X]$, are applied in parallel to M analog mixers which multiply $[X]$ with the random signal $[\phi]$. Each mixer output is then integrated by a low-pass filter, and the output, $[Y]$, is digitized by an ADC. A hardware prototype processed input signals with a bandwidth of 120 MHz. The compressed output was accurately sampled at 280 MHz compared to the Nyquist sampling frequency of 2 GHz. A comparison of RD [16] and MWC [17] is given by Lexa *et al.* [18].

Chen *et al.* [19], [20] recently described digital-domain compressed sensing for EEG and ECG signals [Fig. 12(c)]. The digital CS system first digitizes the conditioned biosignal using a Nyquist rate ADC. A sequence of N samples, $[X]$, is then applied in parallel to an array of M multiply-and-accumulate (MAC) stages to generate the M compressed output samples, $[Y]$. The 8-bit SAR ADC occupies 90×150 μm and 50 16-bit MACs occupy 200×550 μm in 90 nm CMOS. The power dissipation is only 1.9 μW from $V_{dd} = 0.6$ V for EEG signals with 10× to 40× compression factors.

B. Design of the Measurement Matrix

The $M \times N$ measurement matrix, $[\phi]$, is populated with random coefficients for which key parameters include the number of bits, the type of random distribution, the overall structure of the matrix, incoherence with $[\psi]$, etc.

First, consider the effects of random coefficient selection and bit-precision. According to Donoho, Candès and Tao [4]–[6], the measurement matrix can comprise random numbers from Bernoulli, Gaussian, Uniform, etc., distributions. Intuitively, it is expected that the random coefficients will differ in their incoherence to the sampling basis and thus produce different compression results. Simulations have shown for ECG and EMG signals that 6-bit coefficients are needed for Gaussian and Uniform distributions [8], [9].

Another consideration is the structure of the measurement matrix. Although entries of the standard measurement matrix are independently populated with random coefficients, structured $[\phi]$ matrices can save both chip area and power. In particular, the special class of Toeplitz matrices is interesting.

A Toeplitz matrix—one in which every left-to-right diagonal is constant—has the following form:

$$\Phi_{Toeplitz} = \begin{bmatrix} \phi_n & \phi_{n-1} & \cdots & \phi_1 \\ \phi_{n+1} & \phi_n & \cdots & \phi_2 \\ \ddots & \ddots & \ddots & \vdots \\ \phi_{n-1} & \phi_{n-2} & \cdots & \phi_n \end{bmatrix}. \tag{9}$$

The circulant matrix is a derivative of the Toepltz matrix wherein each row is rotated one column to the right relative to the previous row

$$\Phi_{Circulant} = \begin{bmatrix} \phi_n & \phi_{n-1} & \cdots & \phi_1 \\ \phi_1 & \phi_n & \cdots & \phi_2 \\ \ddots & \ddots & \ddots & \vdots \\ \phi_{n-1} & \phi_{n-2} & \cdots & \phi_n \end{bmatrix}. \tag{10}$$

Another potential $[\phi]$ is the triangular matrix wherein all entries above or below the main diagonal are zero

$$\Phi_{Triangular} = \begin{bmatrix} \phi_n & \phi_{n-1} & \cdots & \phi_1 \\ 0 & \phi_n & \cdots & \phi_2 \\ \ddots & \ddots & \ddots & \vdots \\ 0 & 0 & \cdots & \phi_n \end{bmatrix}. \tag{11}$$

Fig. 13 shows $SQNR$ versus C for several 1-bit measurement matrices [21]. The circulant matrix provides superior performance for ECG signals and the use of a 1-bit $[\phi]$ reduces the hardware complexity and saves energy.

C. Dynamic-N

Because the sparsity of a signal changes depending on the duration of observation, allowing N to vary would, in theory, enable dynamic tuning of the sparsity to achieve an optimal ratio between the amount of data transmitted and the reconstruction accuracy. Applying this approach to EMG data, however, shows that the sparsity level is almost independent of N (Fig. 14). Moreover, this approach does not work for relatively periodic signals (e.g., ECG) because the sparsity is approximately constant for any frame longer than the period of the signal. Thus, $N = 1024$ is chosen for the experiments described herein.

VI. CS Signal Reconstruction/Decoder Design

The purpose of the CS decoder [Fig. 4(b)] is to generate a reconstructed version, $\widehat{x}(t)$, of the original biosignal, $x(t)$, using the compressed signal, $y(t)$, the measurement matrix, $[\phi]$ and

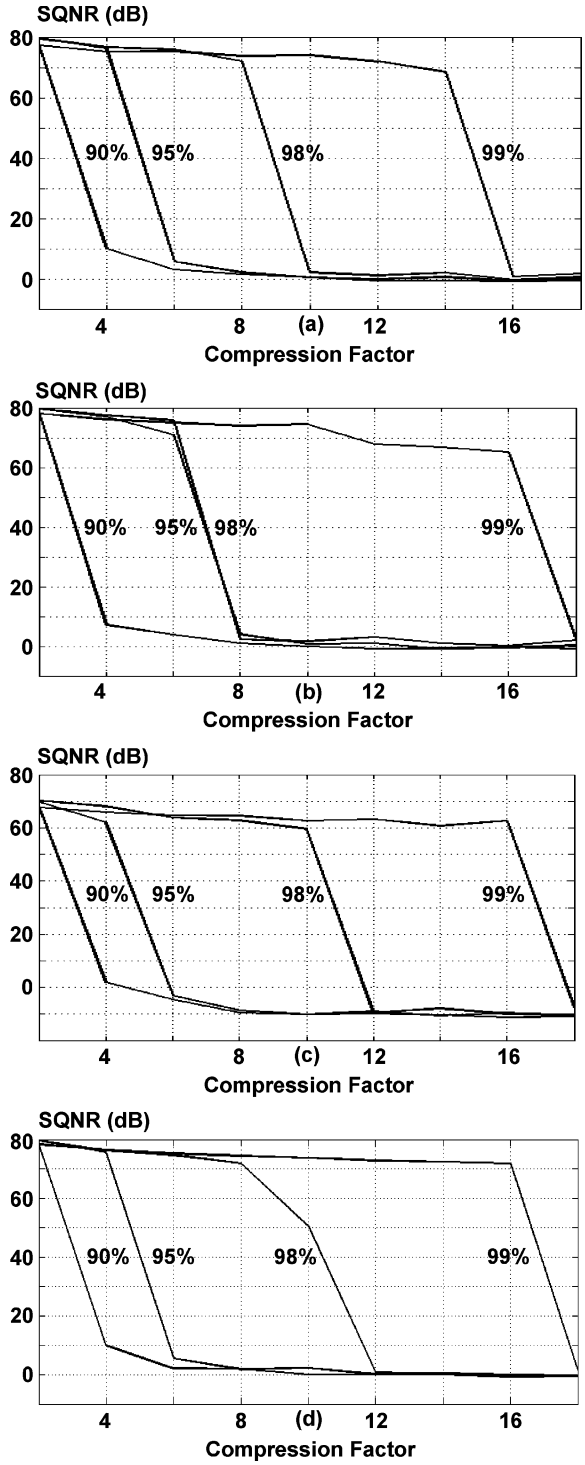

Fig. 13. $SQNR$ versus C for 1-bit measurement matrices for ECG. (a) Bernoulli. (b) Toeplitz (Bernoulli vector). (c) Circulant (Bernoulli vector). (d) Triangular Bernoulli.

the sampling basis, $[\psi]$. Because the CS signal recovery problem is an underdetermined system of linear equations as mentioned earlier, many solutions satisfy $[Y] = [\phi][\widehat{X}]$, but only a few also satisfy the sparsity requirement for $\widehat{x}(t)$. CS usually employs an optimization algorithm to select the sparsest solution as $\widehat{x}(t)$ because it is known to exhibit the lowest error bound [22].

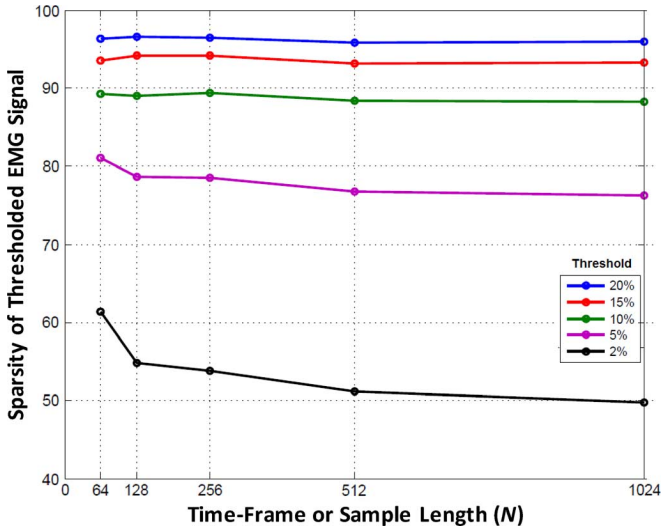

Fig. 14. Sparsity versus sample length for ECG signals.

A. CS Reconstruction Algorithms

The original CS reconstruction algorithm is convex optimization [4]–[6] wherein the L_1-norm of the reconstructed signal, $\|[\widehat{X}]\|_1 = \sum_i |\widehat{x}_i|$, is an efficient measure of sparsity. The CS reconstruction process is described by the following L_1-norm convex optimization:

$$Min\|\hat{X}\|_1 \quad \text{subject to} \quad [Y] = [\Phi][\hat{X}] \tag{12}$$

which can be cast as a linear programming problem. This approach is also known as *basis pursuit*.

In order for signal reconstruction to be robust in the presence of noise, the constraints of the optimization problem are relaxed

$$Min\|\hat{X}\|_1 \quad \text{subject to} \quad \left\|[Y] - [\Phi][\hat{X}]\right\|_2 \leq \varepsilon. \tag{13}$$

The relaxed L_1-norm convex optimization is known as *Least Absolute Shrinkage and Selection Operator* (LASSO).

The results of this section were obtained using the open-source software CVX [23] which solves (12) using a primal-dual interior-point method.

Finally, an alternative approach to the basis pursuit and LASSO solutions is given by an algorithm that finds $[\widehat{X}]$ as

$$Min\left\{\frac{1}{2}\left\|\left([Y] - [\Phi][\hat{X}]\right)\right\|_2^2 + \lambda\left\|[\hat{X}]\right\|_1\right\}. \tag{14}$$

This solution is known as *basis pursuit de-noising* (BPDN) [24], [25]. It finds a solution that simultaneously minimizes the noise level $([Y] - [\phi][\widehat{X}])$ and the sparsity. The parameter λ controls the balance between both optimization objectives.

Unlike convex optimization, greedy algorithms solve the reconstruction problem in a less exact manner by greedily optimizing a metric that predicts error minimization.

Matching pursuit, one class of CS reconstruction greedy algorithms, attempts to find the columns of the measurement matrix $[\phi]$ that have the most participation in the measurement $[Y]$. The column(s) of $[\phi]$ with the strongest correlation to the residual is added to the support vector and its contribution is subtracted from the residual. In *Orthogonal Matching Pursuit* (OMP), only one column of $[\phi]$ is added to the support vector

TABLE II
OVERVIEW OF CS RECONSTRUCTION METHODS

CS Reconstruction Algorithm	Algorithm Objective	Time Complexity
Basis Pursuit Convex Optimization [23]	Search the space for a solution with the min. L_1-norm	$O(M^2N^{1.5})$
Basis Pursuit De-noising (*BPDN*) Convex Optimization [24][25]	Search the space for a solution with minimum error and the min. L_1-norm together	$O(M^2N^{1.5})$
Orthogonal Matching Pursuit (*OMP*) [26]	Find the columns of $[\Phi]$ with the max. correlation to the residual	$O(KMN)$
Compressive Sampling Matching Pursuit (*CoSaMP*) [28]	Find the top $2K$ columns of $[\Phi]$ with the max. correlation to the residual	$O(log(K)MN)$
Normalized Iterative Hard Thresholding (*NIHT*) [29]	Find the top K values of the sum of previous best guess and the signal proxy of the residual	$O(log(K)MN)$

per iteration [26], [27]. In *Compressed Sampling Matching Pursuit* (CoSaMP), the top $2K$ columns of $[\phi]$ are added to the support vector per iteration [28].

Another popular reconstruction algorithm is the *Normalized Iterative Hard Thresholding* (NIHT) algorithm [29]. This method differs from the greedy algorithms described above by not directly searching for the columns of $[\phi]$ that reduce the residual error. Instead it operates by iteratively selecting solutions that both minimize the residual and maximize the difference between the solutions of the current and previous iterations. Table II summarizes key features of the algorithms.

B. CS Reconstruction Performance for ECG Biosignals

The primary focus of this study is to apply CS to biosignal acquisition for efficient, low-power body area networks and to compare reconstruction algorithms for an ECG biosensor.

More than 50 hours of ECG signals were collected from the *Physiobank* database [7]. Because ECG signals show considerable sparsity in time, an identity matrix is used as the sparsifying domain for these experiments. The ECG signal is windowed to 1024 samples, and dynamically thresholded to control sparsity. To account for circuit noise, additive white Gaussian noise (AWGN) was added to the thresholded signal so that the compressed ECG signal exhibited about 80 dB SNR (typical of an ECG sensor analog front-end). Compression was achieved using a 6-bit 256×1024 Gaussian $[\phi]$ matrix (i.e., $C = 4$). Reconstruction was performed in *MATLAB*.

The high sparsity levels needed for exact recovery are not guaranteed at reconstruction because of noise. Thus, a realistic measure of recovery accuracy is the estimation SNR

$$SNR = 20\,log_{10}\left\{\frac{\|[X]\|_2}{\left\|[X]-[\hat{X}]\right\|_2}\right\}. \qquad (15)$$

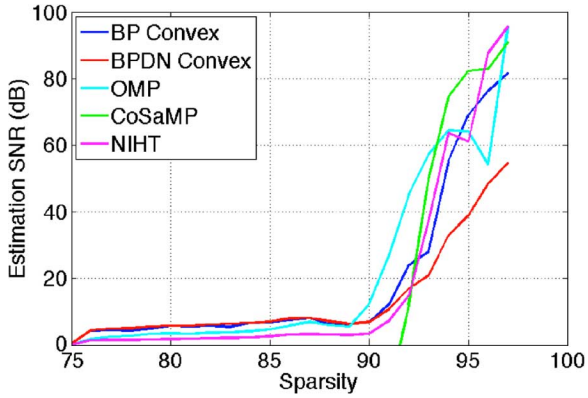

Fig. 15. ECG signal reconstruction accuracy.

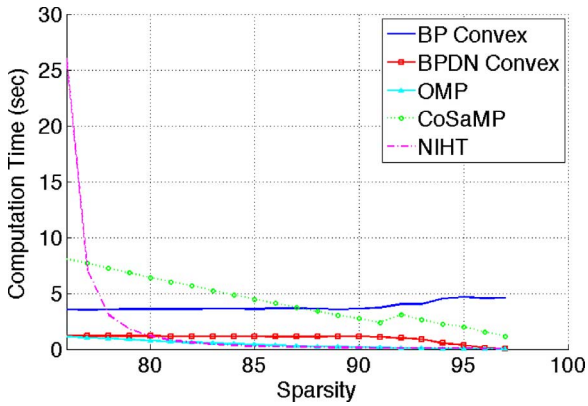

Fig. 16. ECG signal reconstruction computation time.

Fig. 15 compares the accuracy of several CS reconstruction methods for ECG signals. All reconstruction algorithms except $BPDN$ meet the target SNR level (80 dB) at high sparsity levels. OMP shows higher accuracy at lower sparsity levels but its reliability is of concern because the performance dips at high sparsity levels. $CoSaMP$ shows high accuracy at lower sparsity levels with better reliability.

Computation time is also an important factor in a CS decoder because it has a direct impact on energy efficiency and real-time application feasibility. The computation times of these algorithms are compared in Fig. 16. OMP requires the least computation time. BP convex optimization has higher computational complexity than most greedy solutions but is notably independent of sparsity. $CoSaMP$ shows the largest computation time of the greedy solutions, but improves at higher sparsity levels (>90%) where the CS reconstruction algorithms show consistent recovery (Fig. 15).

C. CS Reconstruction Performance for EMG Biosignals

Several EMG signals recordings, which exhibit sparsity in both the time and frequency domains, were collected from the *Physiobank* [7] for healthy, myopathy and neuropathy patients. Fig. 11 shows the sparsity for various thresholding levels for the different EMG signals in both time and frequency. Healthy EMG signals exhibit sparsity in both domains; however, neuropathy signals exhibit sparsity in time only whereas myopathy

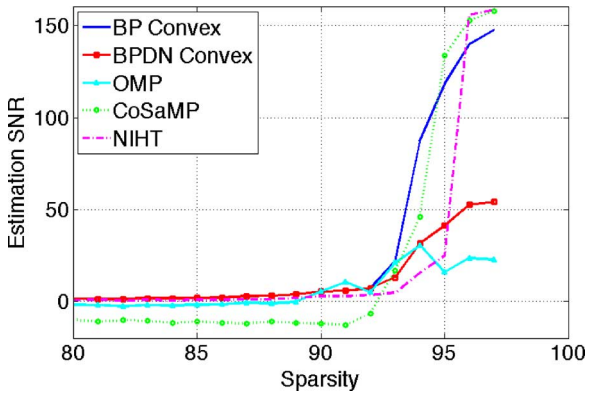

Fig. 17. EMG time-domain signal reconstruction accuracy.

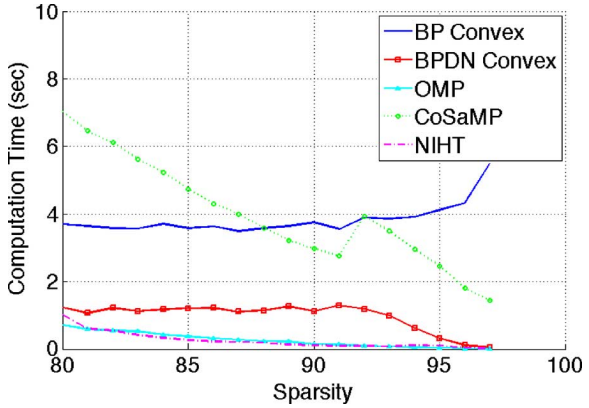

Fig. 18. EMG time-domain signal reconstruction computation time.

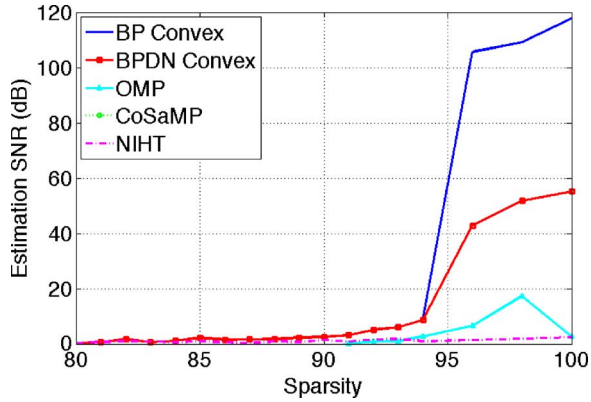

Fig. 19. EMG frequency-domain signal reconstruction SNR.

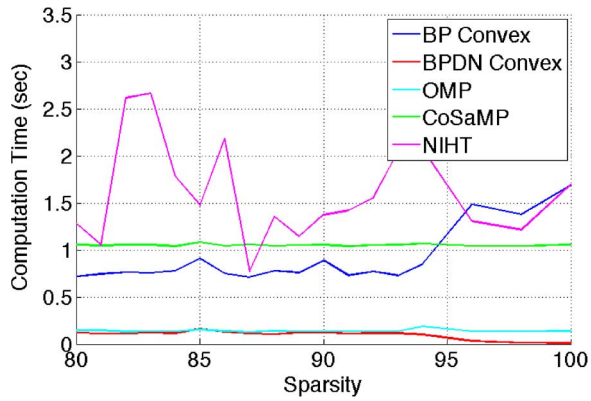

Fig. 20. EMG frequency-domain signal reconstruction computation time.

signals are sparse in frequency only. As such, CS reconstruction is examined for both domains.

CS was applied to EMG signals in the time domain windowed to 1024 samples and dynamically thresholded at 10% to control the sparsity. To account for circuit and sampling noise, AWGN was added so that the compressed EMG signal achieved $SNR = 80$ dB. Compression was performed using a 6-bit 256 $\times$ 1024 Gaussian $[\phi]$ matrix with reconstruction via *MATLAB*.

Fig. 17 compares the reconstruction accuracy for time-domain signals. BP convex, $CoSaMP$ and $NIHT$ meet the SNR goal at high sparsity (>95%) whereas $BPDN$ convex and OMP do not successfully reconstruct the EMG signals.

Fig. 18 compares the computation times of the CS reconstruction algorithms applied to the EMG time-domain signals. BP convex optimization has higher computational complexity than most of the greedy solutions but is notably independent of sparsity up to the 96% level, beyond which it surprisingly increases. $CoSaMP$ shows the greatest computation time of the greedy algorithms, but approaches the other solutions at higher sparsity levels (>90%) where the CS reconstruction shows successful recovery. OMP and $NIHT$ are the fastest algorithms.

Finally, CS was applied to EMG signals in the frequency domain. BP convex (Fig. 19) exhibits superior performance whereas OMP, $CoSaMP$ and $NIHT$ fail reconstruction.

Fig. 20 compares the computation times of the reconstruction algorithms applied to EMG frequency-domain signals. BP convex optimization has higher computational complexity but is notably independent of sparsity. $CoSaMP$ and $NIHT$ are the slowest of the greedy solutions. OMP and $BPDN$ convex optimization are the fastest.

VII. Conclusions

Several design considerations for CS acquisition systems for ECG and EMG biosignals are presented. Dynamic thresholding is used to tradeoff sparsity versus accuracy and is shown to be reliable over difficult biosignal morphologies. Experimental results show that a 1-bit Bernoulli measurement matrix is capable of producing up to 16$\times$ compression for ECG and EMG biosignals. Finally, state-of-the-art CS encoder architectures are surveyed and CS signal reconstruction algorithms are compared.

References

[1] E. Jovanov, A. Milenkovic, C. Otto, and P. de Groen, "A wireless body area network of intelligent motion sensors for computer assisted physical rehabilitation," *J. NeuroEng. Rehabil.*, vol. 2, pp. 1–10, Mar. 2005.

[2] J. Pandey and B. Otis, "A sub-100 μW MICS/ISM band transmitter based on injection-locking and frequency multiplication," *IEEE J. Solid-State Circuits*, vol. 46, pp. 1049–1058, May 2011.

[3] H. Garudadri, P. Baheti, S. Majumdar, C. Lauer, F. Masse, J. van de Molengraft, and J. Penders, "Artifacts mitigation in ambulatory ecg telemetry," in *Proc. IEEE Int. Conf. e-Health Networking Applications and Services*, 2010, pp. 338–344.

[4] D. L. Donoho, "Compressed sensing," *IEEE Trans. Inf. Theory*, vol. 52, pp. 1289–1306, Sep. 2006.

[5] E. Candés and T. Tao, "Near optimal signal recovery from random projections: Universal encoding strategies," *IEEE Trans. Inf. Theory*, vol. 52, pp. 5406–5425, Dec. 2006.

[6] E. Candés, "An introduction to compressive sampling," *IEEE Signal Process. Mag.*, vol. 25, pp. 21–30, Mar. 2008.
[7] A. Goldberger *et al.*, "Physiobank, PhysioToolkit, and PhysioNet: Components of a new research resource for complex physiological signals," *Circulation*, vol. 101, no. 23, pp. 1–6, 2000.
[8] E. G. Allstot, A. Y. Chen, A. M. R. Dixon, D. Gangopadhyay, and D. J. Allstot, "Compressive sampling of ECG bio-signals: Quantization noise and sparsity considerations," in *Proc. IEEE Biomedical Circuits and Systems Conf.*, Nov. 2010, pp. 41–44.
[9] A. Salman, E. G. Allstot, A. Y. Chen, A. M. R. Dixon, D. Gangopadhyay, and D. J. Allstot, "Compressive sampling of EMG bio-signals," in *Proc. IEEE Int. Symp. Circuits and Systems*, May 2011, pp. 2095–2098.
[10] R. Dorfman, "The detection of defective members of large populations," *Ann. Math. Stat.*, vol. 14, no. 4, pp. 436–440, Dec. 1943.
[11] M. Sobel and P. A. Groll, "Group testing to eliminate efficiently all defectives in a binomial sample," *Bell Syst. Tech. J.*, vol. 38, no. 5, pp. 1179–1252, Sep. 1959.
[12] R. Rieger and J. T. Taylor, "An adaptive sampling system for sensor nodes in body area networks," *IEEE Trans. Neural Syst. Rehabil. Eng.*, vol. 17, pp. 183–189, Mar. 2009.
[13] R. F. Yazicioglu, S. Kim, T. Torfs, H. Kim, and C. Van Hoof, "A 30 μW analog signal processor ASIC for portable biopotential signal monitoring," *IEEE J. Solid-State Circuits*, vol. 46, pp. 209–223, Jan. 2011.
[14] R. R. Harrison, "A low-power integrated circuit for adaptive detection of action potentials in noisy signals," in *Proc. Int. Conf. IEEE Engineering in Medicine and Biology Society*, Sept. 2003, pp. 3325–3328.
[15] J. N. Laska, S. Kirolos, M. F. Duarte, T. S. Ragheb, R. G. Baraniuk, and Y. Massoud, "Theory and implementation of an analog-to-information converter using random demodulation," in *Proc. IEEE Int. Symp. Circuits and Systems*, 2007, pp. 1959–1962.
[16] T. Ragheb, J. N. Laska, H. Nejati, S. Kirolos, R. G. Baraniuk, and Y. Massoud, "A prototype hardware for random demodulation based compressive analog-to-digital conversion," in *Proc. IEEE Midwest Symp. Circuits and Systems*, Aug. 2008, pp. 37–40.
[17] M. Mishali, Y. C. Eldar, O. Dounaevsky, and E. Shoshan, "Xampling: Analog to digital at Sub-Nyquist rates," *IET Circuits, Devices Syst.*, vol. 5, pp. 8–20, Jan. 2011.
[18] M. A. Lexa, M. E. Davies, and J. S. Thompson, "Reconciling compressive sampling systems for spectrally sparse continuous-time signals," *IEEE Trans. Signal Process.*, vol. 60, pp. 155–171, Jan. 2012.
[19] F. Chen, A. P. Chandrakasan, and V. Stojanović, "A signal-agnostic compressed sensing acquisition system for wireless and implantable sensors," in *Proc. IEEE Custom Integrated Circuits Conf.*, 2010, pp. 1–4.
[20] F. Chen, A. P. Chandrakasan, and V. Stojanović, "Design and analysis of a hardware-efficient compressed sensing architecture for data compression in wireless sensors," *IEEE J. Solid-State Circuits*, vol. 47, pp. 744–756, Mar. 2012.
[21] E. G. Allstot, A. Y. Chen, A. M. R. Dixon, D. Gangopadhyay, H. Mitsuda, and D. J. Allstot, "Compressed sensing of ECG bio-signals using one-bit measurement matrices," in *Proc. IEEE Int. NEWCAS Conf.*, 2011, pp. 213–216.
[22] E. Candés, J. Romberg, and T. Tao, "Stable signal recovery from incomplete and inaccurate measurements," *Commun. Pure Appl. Math.*, vol. 59, pp. 1207–1223, Aug. 2006.
[23] M. Grant *et al.*, CVX: MATLAB Software for Disciplined Convex Programming ver. 1.21 [Online]. Available: http://cvxr.com/cvx
[24] S. S. Chen, D. L. Donoho, and M. A. Saunders, "Atomic decomposition by basis pursuit," *SIAM J. Sci. Comput.*, vol. 20, pp. 33–61, Jan. 1999.
[25] W. Lu and N. Vaswani, "Modified basis pursuit denoising (modified-BPDN) for noisy compressive sensing with partially known support," in *Proc. IEEE Int. Conf. Acoustics Speech and Signal Processing*, 2010, pp. 3926–3929.
[26] J. A. Tropp and A. C. Gilbert, "Signal recovery from random measurements via orthogonal matching pursuit," *IEEE Trans. Inf. Theory*, vol. 53, pp. 4655–4666, Dec. 2007.
[27] T. Blumensath and M. E. Davies, On the Difference Between Orthogonal Matching Pursuit and Orthogonal Least Squares, Univ. of Edinburgh, Mar. 2007, Tech. Rep.
[28] D. Needell and J. A. Tropp, "COSAMP: Iterative signal recovery from incomplete and inaccurate samples," *Appl. Comput. Harmon. Anal.*, vol. 26, pp. 301–321, Apr. 2008.
[29] T. Blumensath and M. E. Davies, "Normalized iterative hard thresholding: Guaranteed stability and performance," *IEEE J. Sel. Topics Signal Process.*, vol. 4, pp. 298–309, Mar. 2010.
[30] S. Hwang, M. Trakimas, and S. Sonkusale, "A low-power asynchronous ECG acquisition system in CMOS technology," in *Proc. IEEE Int. Conf. Engineering and Medicine in Biology*, 2010, pp. 5262–5265.
[31] R. Agarwal and S. R. Sonkusale, "Input-feature correlated asynchronous analog-to-information converter for ECG monitoring," *IEEE Trans. Biomed. Circuits Syst.*, vol. 5, no. 5, pp. 459–467, Oct. 2011.

Anna M. R. Dixon (S'05) received the B.S. degree in 2006 and the M.S. degree in 2008 from The Ohio State University, Columbus, in 2006 and 2008, respectively.

Currently, she is pursuing the Ph.D. degree in electrical engineering at the University of Washington, Seattle. Her research interests include low-power biomedical instrumentation, circuits and systems design, and compressed sensing. She was awarded an Intel/SRCEA Master's Scholarship from 2006–2008 and since 2011 she has held an Intel/SRCEA Graduate Fellowship. She received the Analog Devices Inc. Outstanding Student Analog Designer Award in 2011.

Emily G. Allstot (S'10) is currently pursuing the B.S. degree in electrical engineering at the University of Washington (UW), Seattle.

Her research interests include analog circuits and systems, biomedical instrumentation, and compressed sensing. She was awarded an Undergraduate Research Opportunities (URO) Scholarship from the Semiconductor Research Corporation in 2011–2012. She currently serves as the Public Relations Officer for the UW IEEE Student Branch and as a 2012 summer intern at Texas Instruments Incorporated, Santa Clara, CA.

Daibashish Gangopadhyay (S'06–M'11) received the B.S. (Hons.) and M.S. degrees in electronics and electrical communication engineering from the Indian Institute of Technology, Kharagpur, India, in 2005 and 2006, respectively, and the Ph.D. degree from the University of Washington, Seattle, in 2011.

During 2008–2009 he was an intern with the Qualcomm Research Center, San Diego, CA, where he worked on biomedical sensor circuits for personal area network applications. Since 2011, he has been with the RF-Analog Group, Marvell Semiconductor Inc., Santa Clara, CA. His research interests include CMOS frequency synthesizers, software-defined radio receivers, RF and analog front-ends for biomedical sensor applications, and compressed sensing. He received the Analog Devices Outstanding Student Designer Award in 2010 and an IEEE RFIC Symposium Best Student Paper Award in 2011.

David J. Allstot (S'72–M'72–SM'83–F'92) received the B.S. degree from the University of Portland, Portland, OR, the M.S. degree from Oregon State University, Corvallis, and the Ph.D. degree from the University of California, Berkeley.

He has held several industrial and academic positions and has been the Boeing-Egtvedt Chair Professor of Engineering at the University of Washington since 1999. He was Chair of the Department of Electrical Engineering from 2004 to 2007. He is currently a Visiting Professor in the Department of Electrical Engineering, Stanford University, Stanford, CA. He has advised approximately 100 M.S. and Ph.D. graduates and authored about 275 papers.

Dr. Allstot has received several outstanding teaching and advising awards. His awards include the 1978 IEEE W. R. G. Baker Prize Paper Award, 1995 and 2010 IEEE Circuits and Systems Society (CASS) Darlington Best Paper Awards, 1998 IEEE International Solid-State Circuits Conference (ISSCC)

Beatrice Winner Award, 1999 IEEE CASS Golden Jubilee Medal, 2004 Technical Achievement Award of the IEEE CASS, the 2005 Aristotle Award of the Semiconductor Research Corporation, the 2008 University Research Award of the Semiconductor Industries Association, and the 2011 IEEE CASS Mac Van Valkenburg Award. His service includes: 1990–1993 Associate Editor of the IEEE TRANSACTIONS ON CIRCUITS AND SYSTEMS II, 1993–1995 Editor of IEEE TRANSACTIONS ON CIRCUITS AND SYSTEMS II, 1990–1993 Member Technical Program Committee of the IEEE CICC Conference, 1992–1995 Member, Board of Governors of IEEE CASS, 1994–2004 Member, Technical Program Committee of IEEE ISSCC, 1996–2000 Member, Executive Committee of IEEE ISSCC, 1996–2000 Short Course Chair of IEEE ISSCC, 2000–2001 Distinguished Lecturer of IEEE CASS, 2001 Co-General Chair of IEEE ISCAS, 2006 Member, Aristotle Award Committee, Semiconductor Research Corporation, 2006–2007 Distinguished Lecturer, IEEE SSCS, 2007 Member, Kirchhoff Award Committee, IEEE, 2008 General Co-Chair of IEEE ISCAS, and 2009 President of IEEE Circuits and Systems Society.